

Stability Criteria for Two-Dimensional Wetting in Monolayers

P. Heinig,[†] S. Wurlitzer,[†] Th. John,[‡] and Th. M. Fischer^{*,†}

Max Planck Institute of Colloids and Interfaces, Am Mühlenberg 1, D-14476 Golm, Germany, and
Fakultät für Physik und Geowissenschaften, Universität Leipzig, Linnéstrasse 5, 04103 Leipzig, Germany

Received: January 15, 2002; In Final Form: August 19, 2002

Two-dimensional pendant liquid expanded droplets partially wet the liquid condensed/gas-phase boundaries in methyl octadecanoate Langmuir monolayers. Their shape is described by the Young–Laplace equation including long-range electrostatic interactions on a scale Δ . It is invariant under shape-invariant scale transformations. We show that the local stability at the three-phase intersection point is described by Young's equation for the contact angle. The contact angle is not invariant under shape-invariant scale transformations but is a materials constant at a fixed scale parameter Δ . By comparison of numerically simulated droplets with experimental droplets observed with a fluorescence microscope, we determine the spreading coefficient of wetting Langmuir monolayer phases as well as a lower limit for Δ . We find $0.12 \mu\text{m} < \Delta$ and suggest that the scale parameter shall be interpreted as a dipolar correlation length, not as a molecular cutoff length.

1. Introduction

Wetting is a universal physical concept with growing significance in basic research and modern technology. The main question dealing with wetting is whether and in which morphology a substance is thermodynamically stable on a given substrate.¹ Although wetting has been studied for about 200 years,² important questions still remain unanswered. Especially, the effect of long-range interactions on pattern formation in self-assembling systems is a feature of recent basic research^{3–7} and is of enormous interest in biology and technology.

A Langmuir monolayer is a suitable system for studying wetting in the presence of long-range interactions. It is a 2D system of amphiphiles on the air/water interface, and several phases according to the positional or rotational order of the molecules occur. In the three-phase coexistence region of a gaseous (G), liquid expanded (LE), and liquid-condensed (LC) phase, 2D wetting phenomena are observed. Typical shapes of LE droplets partially wetting a LC/G boundary are shown in Figure 1. The characteristic droplet shapes within the monolayer are caused by electrostatic forces between the molecules deforming larger droplets in a specific way, while leaving the smaller droplet shapes approximately in a circular segment shape. In contrast to 3D systems, dipole–dipole forces between the molecules are not screened, and the resulting long-range interaction characterized by the surface potentials of the monolayer phases has been shown to be responsible for a rich variety of monolayer patterns. Wetting instabilities in Langmuir monolayers⁸ might be of interest in intramembrane biochemical reactions associated with changes in membrane potentials, which also play an important role in cell signal transduction.^{9–12}

Here we report on 2D wetting in a methyl octadecanoate monolayer (Figure 1). We theoretically study thermodynamic stability criteria for 2D wetting dipolar droplets with respect to

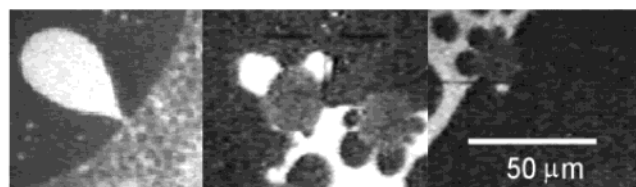


Figure 1. Droplets observed using fluorescence microscopy in the three-phase coexistence region of a methyl octadecanoate monolayer (LE: bright areas, G: black, LC: gray) with different droplet areas of $A = 8.9 \times 10^{-10} \text{ m}^2$, $2.0 \times 10^{-10} \text{ m}^2$, $0.7 \times 10^{-10} \text{ m}^2$, and $0.1 \times 10^{-10} \text{ m}^2$. The droplet shapes depend on their sizes.

the different wetting modes (complete or partial wetting). A simple theoretical model allows us to exclude the interpretation of the observed droplets as completely wetting droplets without a three-phase intersection point. We show that for the partial wetting case the contact angle between the interface lines is determined by Young's law. Furthermore, we find theoretical droplet shapes by a numerical iteration procedure and determine the spreading coefficient of methyl octadecanoate monolayer phases by comparison of these droplets with fluorescence images of experimentally observed droplets. Local stability criteria at the three-phase intersection point restrict the scaling parameter Δ to be larger than the minimum value $\Delta_{\text{min}} = 0.12 \mu\text{m}$. The latter implies that Δ has to be interpreted as a dipolar healing length rather than a molecular separation.

2. Theory

2.1. Equilibrium Conditions. The common model^{13–18} separates long- and short-range interactions by introducing a bare¹⁹ line tension, the line tension in the limit of vanishing dipolar interaction. This line tension is a materials parameter and is constant in the three-phase coexistence region (new perceptions show that this theory may be too simple in some cases²⁰). The total free energy of the monolayer can be written

* Corresponding author. E-mail: thomas.fischer@mpikg-golm.mpg.de.

[†] Max Planck Institute of Colloids and Interfaces.

[‡] Universität Leipzig.

as the sum of the long-range electrostatic energy F_{el} , line energy F_{λ} , and the 2D bulk energy F_0 :

$$F = F_{\text{el}} + F_{\lambda} + F_0 \quad (1)$$

with the long-range electrostatic energy

$$F_{\text{el}} = \sum_{ij} \frac{\mu_i \mu_j}{2} \int_{A_i} \int_{A_j} \frac{dA dA'}{\sqrt{(\mathbf{r} - \mathbf{r}')^2 + \Delta^2}^3} \quad (2)$$

The summation is performed over all monolayer domains i and j with integration over the areas A_i and A_j . The quantity μ_i is defined via surface potentials V_i of the phase (of domain) i as

$$\mu_i^2 = \frac{\epsilon_0}{4\pi} \frac{2\epsilon_w \epsilon_{\text{air}}}{\epsilon_w + \epsilon_{\text{air}}} (V_i - \bar{V})^2 \quad \text{and} \quad \mu_{ij} = \mu_i - \mu_j \quad (3)$$

where $\epsilon_0 = 8.854 \text{ pN/V}^2$ is the vacuum permittivity and ϵ_w and ϵ_{air} are the relative permittivities of water and air. $\bar{V} = \sum_i A_i V_i / \sum_i A_i$ is a reference potential chosen as the area average.

For large distances between the area elements dA and dA' , the integrand in eq 2 is approximately $1/(\mathbf{r} - \mathbf{r}')^3$ (i.e., the energy between two dipoles perpendicular to the surface). The length Δ prevents the dipole energy from diverging at $\mathbf{r} - \mathbf{r}' = 0$. Its physical meaning is the cutoff length of the dipole interaction, the length scale on which short-range interactions become more important than the dipole interaction. The short-range attraction might be van der Waals forces with the range of nanometers. In the literature,^{13,14,21} the cutoff length is usually set to the distance between the molecules on the order of angstroms.²²

A more abstract interpretation of Δ is as a scale parameter in general. Note that Δ is the only characteristic length scale in eq 2. The scale parameter separates the long-range interaction described by the integral eq 2 and the short-range interactions all represented by the bare line tensions. The choice of the scale parameter is (almost) arbitrary, and the macroscopic physics (shapes of domains) remains unchanged when switching from one set of model parameters $(\tilde{\mu}_1, \Delta_1, \lambda_1, p_1)$ to another $(\tilde{\mu}_2, \Delta_2, \lambda_2, p_2)$ that is connected to the first set via a shape-invariant scale transformation to be discussed in the next section. Note that the bare line tension λ_{ij} (of the interface between phases i and j) has no meaning without stating the corresponding scale Δ .²²

The other terms in eq 1 are

$$F_{\lambda} = \sum_{\{ij\}} \lambda_{ij} \int_0^{p_{ij}} ds_{ij} \quad \text{and} \quad F_0 = \sum_i F_0^i(A_i) \quad (4)$$

The bulk free energy F_0 is independent of the shapes of the domains and depends solely on the areas occupied by the individual phases.

Minimizing the free energy while varying the droplet shape and the position of the three-phase intersection points under the constraint of a constant droplet area directly yields the local stability criteria for the shape and contact angle (Appendices A and B). One finds that the product of the line tension λ_{ij} and the curvature $\kappa_{ij}(\mathbf{r})$ on the interface between phases i and j for a point on the droplet interface \mathbf{r} is proportional to the pressure difference across the phase boundary:^{24,25}

$$\lambda_{ij} \kappa_{ij}(\mathbf{r}) = p_{ij} + p_{\text{el}}(\mathbf{r}) \quad (5)$$

This equation is similar to the Young–Laplace equation describing the shape of 3D droplets in the gravitation field²⁶ with the Laplace pressure p_{ij} and the dipole pressure p_{el} instead of the gravity pressure:

$$p_{\text{el}}(\mathbf{r}) = - \sum_k \mu_{ij} \mu_k \int_{A_k} \frac{dA'}{\sqrt{(\mathbf{r} - \mathbf{r}')^2 + \Delta^2}^3} \quad (6)$$

The dipole pressure causes the typical pendant droplet shape. The 2D Young–Laplace equation can be used to measure the bare line tension by pendant droplet tensiometry. Experiments of this kind have been performed for the LE/G interface of a methyl octadecanoate monolayer.²⁵

For the special case of a liquid (LE) droplet in gas (G) partially wetting a solidlike substrate (LC), one finds for the contact angle α the well-known Young condition (Appendix B):

$$\cos \alpha = \frac{\lambda_{\text{LC/G}} - \lambda_{\text{LC/LE}}}{\lambda_{\text{LE/G}}} \quad (7)$$

For any Δ , the contact angle is a materials constant and does not depend on the droplet shape or size or the structure of the surroundings.

2.2. Scaling Laws. 2.2.1. Shape-Invariant Scale Transformations. As described in refs 14, 24, and 25, the 2D Young–Laplace law for shapes with decent curvature is invariant to the application of the scale transformation (Appendix C):

$$(\Delta_1, \lambda_{ij,1}, p_1, \mu_{i,1}) \rightarrow (\Delta_2, \lambda_{ij,2}, p_2, \mu_{i,2}) \quad (8)$$

where

$$\begin{aligned} \lambda_{ij,2} &= \lambda_{ij,1} - \mu_{ij,1}^2 \ln \frac{\Delta_2}{\Delta_1} \\ p_2 &= p_1 - (\mu_{i,1}^2 - \mu_{j,1}^2) \left(\frac{\pi}{\Delta_2} - \frac{\pi}{\Delta_1} \right) \quad \text{and} \\ \mu_{i,2} &= \mu_{i,1} \end{aligned}$$

provided Δ_1 and Δ_2 are smaller than then the curvature radius $R = 1/\kappa_{ij}$:

$$\Delta \kappa_{ij} \ll 1 \quad (9)$$

Let us apply the scale transformation (eq 8) to an LE droplet in G partially wetting an LC wall. Using Young's eq 7 for the initial and rescaled droplet, we find that the contact angle is changed. Therefore, the shape of the partially wetting droplet close to the three-phase intersection point cannot be invariant under the scale transformation. This is not surprising since the curvature κ of the droplet exhibits a singularity at the three-phase intersection point, and hence eq 9 is violated. By eliminating the LC/LE and LC/G line tensions in both Young equations, one finds the contact angle rescaling under the shape-invariant scale transformation (eq 8):

$$\alpha_1 \rightarrow \alpha_2 = \arccos \frac{\tilde{\lambda}_{\text{LE/G},1} \cos \alpha_1 - (2 - \tilde{\mu}) \ln \frac{\Delta_2}{\Delta_1}}{\tilde{\lambda}_{\text{LE/G},1} - \tilde{\mu} \ln \frac{\Delta_2}{\Delta_1}} \quad (10)$$

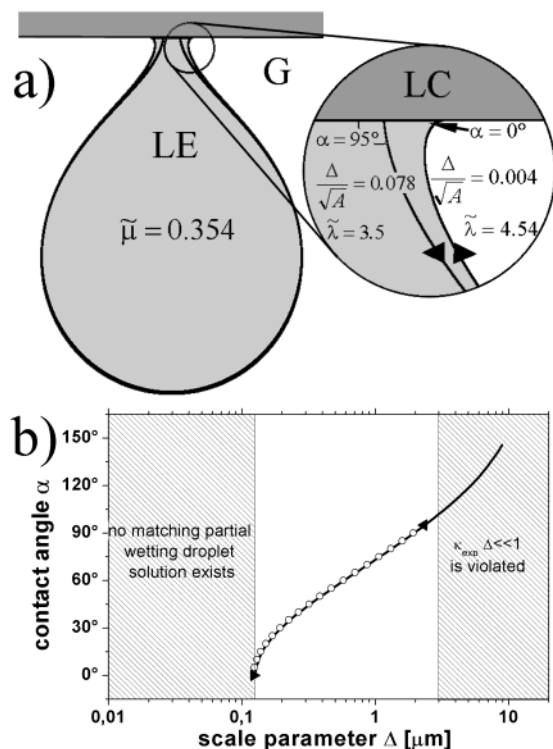


Figure 2. (a) Numerical solutions of the Young–Laplace eq 5 fitted to the largest experimental droplet in Figure 1, demonstrating the shape invariance of the droplet under shape-invariant scale transformations (eq 8) far away from the LC/G boundary. Close to the wall (at distances on the order Δ), the droplet shape is not invariant. It ends at the wall with a scale-parameter-dependent contact angle described by eq 10. The parameter sets ($\tilde{\mu} = 0.354$, $\Delta_1/\sqrt{A} = 0.078$, $\alpha_1 = 95^\circ$, $\tilde{\lambda}_1 = 3.5$) and ($\tilde{\mu} = 0.354$, $\Delta_2/\sqrt{A} = 0.004$, $\alpha_2 = 0^\circ$, $\tilde{\lambda}_2 = 4.45$) of both numerical solutions are related by a shape-invariant scale transformation. (b) Fits (○) of the contact angle to the large experimental droplet in Figure 1 with different scale parameters $0.12 \mu\text{m} < \Delta < 2.3 \mu\text{m}$ using bare line tensions related by shape-invariant scale transformations. The shapes in the entire Δ range lie between the extremal shapes (solid triangle with left-facing base $\hat{=} \Delta = 0.12 \mu\text{m}$ and solid triangle with right-facing base $\hat{=} \Delta = 2.3 \mu\text{m}$) presented in part a. The fitted contact angles agree well with those calculated via eq 10 (—), which is a check for the reliability of the numerics. With increasing scale parameter Δ , the wetting mode changes from partial wetting to partial dewetting. For $\Delta < 0.12 \mu\text{m}$, one finds no partial wetting numerical solution fitting the experimental droplet. For $\Delta > 2.3 \mu\text{m}$, Δ is in the range of the radius of curvature of the experimental droplet, and the shape invariance fails on the experimental observable resolution.

with the dimensionless line tension

$$\tilde{\lambda}_{\text{LE/G}} = \frac{\lambda_{\text{LE/G}}}{\mu_{\text{LE/G}} \mu_{\text{LC/G}}} \quad (11)$$

and the dimensionless surface potential parameter

$$\tilde{\mu} = \frac{\mu_{\text{LE/G}}}{\mu_{\text{LC/G}}} \quad (12)$$

In Figure 2a, two numerical solutions of the Young–Laplace equation fitting the partially wetting droplet of size $A = 890 (\mu\text{m})^2$ in Figure 1 are shown. The numerical solutions correspond to two different sets of model parameters ($\tilde{\mu}_1 = 0.354$, $\Delta_1/\sqrt{A} = 0.078$, $\alpha_1 = 95^\circ$, $\tilde{\lambda}_1 = 3.5$) and ($\tilde{\mu}_2 = 0.354$, $\Delta_2/\sqrt{A} = 0.004$, $\alpha_2 = 0^\circ$, $\tilde{\lambda}_2 = 4.45$) connected via the shape-invariant scale transformation (eq 8). The numerical solutions are the exact solutions to the corresponding set of parameters, and no

use of the shape-invariant scale transformation is made in the numerical treatment. The solutions presented are therefore exact also in those regions close to the three-phase intersection points, where the shape invariance does not hold. As one can see, the shape of both droplets is the same, with deviations occurring only in the vicinity of the LC wall (distances to the wall smaller than Δ). The deviations of both solutions close to the LC wall are such that their contact angles with the LC wall differ in exactly the way predicted by contact-angle scaling law (eq 10). Note that if one decreases the scale parameter Δ below the optical resolution, the deviations of the shapes occur in a region so close to the wall that under experimental conditions they are impossible to resolve. In Figure 2b, fits of the contact angle to the experimental droplet with $A = 890 (\mu\text{m})^2$ with numerical solutions on different scales Δ/\sqrt{A} are shown. The fitted contact angles agree well with the theoretical prediction (eq 10). That we obtain agreement of the shapes far away from the boundary for droplets with different parameters connected by shape-invariant scale transformations subject to different initial conditions (contact angles) is a strong check for both the correct numerical and analytical treatment of the problem.

2.2.2. Contact-Angle-Invariant Scale Transformation.

Young's eq 7 involves only the bare line tensions. Consequently, the contact angle is invariant to a scale transformation, which leaves the bare line tensions unchanged:

$$(\Delta_1/\sqrt{A_1}, \lambda_{ij,1}, \mu_{i,1}) \rightarrow (\Delta_2/\sqrt{A_2}, \lambda_{ij,2}, \mu_{i,2}) \quad (13)$$

where

$$\lambda_{ij,2} = \lambda_{ij,1} \quad \text{and} \quad \mu_{i,2} = \mu_{i,1}$$

A scale transformation of this type does change the shape of a droplet. The physical relevance of this scale transformation is to describe the changes in the shape of a droplet with its size. Since all droplets of different sizes should have the same bare line tension, their contact angles must be the same, whereas their shapes change. Experiments with droplets of different sizes are presented in the next section.

3. Experiment

Methyl octadecanoate from Sigma-Aldrich and 1 mol % of the fluorescence dye nitrobenzoxadiazol-hexadecylamin (NBD-HDA) from Molecular Probes were spread on pure Millipore water (Milli Q) from chloroform solution. The spreading was performed at a temperature of $T = 27.5^\circ\text{C}$ over an area of $A_{\text{mol}} \approx 40 \text{ \AA}^2/\text{molecule}$. The Langmuir trough is equipped with moveable barriers and heating devices, so the area per molecule and the temperature can be varied.²⁷ The monolayer was observed using fluorescence microscopy.²⁸

Under these conditions, the three phases G, LE, and LC coexist, and wetting LE droplets on LC interfaces in a gaseous environment are observed. Figure 1 shows four such droplets of different sizes and shapes. Small droplets ($A < 10^{-10} \text{ m}^2$) resemble a circular segment shape, whereas larger droplets $A > 10^{-10} \text{ m}^2$ are no longer convex and exhibit an inflection point. The largest droplet $A = 8.9 \times 10^{-10} \text{ m}^2$ shows a characteristic throat close to the LC wall, with a minimum thickness at a separation of approximately $2\text{--}3 \mu\text{m}$ from the LC wall.

4. Droplet Fitting

Experimental droplets usually have droplet sizes ranging between 10 and $10^4 (\mu\text{m})^2$, and the positions of droplet interface

lines or three-phase intersection points can be measured with an accuracy of about $\pm 1 \mu\text{m}$. In section 2.2, we have proven the shape invariance to hold for pendant LE droplets for all separations of the droplet interface from the wall larger than Δ . In the following discussion, we will no longer vary Δ to fit the droplets but will make use of the shape-invariant scale transformation. We arbitrarily fix the Δ in the numerics to some value. As long as the chosen Δ is smaller than the resolution of the experimental image, all Δ 's describe the same experimental droplet equally well (cf. shape-invariant scaling). The calculation of the integrals in the Young–Laplace eq 5 numerically is most efficient on a scale that contains only the measurable information of the monolayer structure, so for a numerical treatment, the scale of the optical resolution ($\Delta \approx 1 \mu\text{m}$) is the most efficient. If we are interested in the best fit to the experimental droplet for a different Δ , the answer is that the best fit at the other Δ is obtained via a shape-invariant scale transformation (eqs 8 and 10) from one Δ toward the other.

The measurement of the contact angle directly on the fluorescence image of the droplet is problematic because the contact point is noisy and, as the scaling law (eq 10) implies, the contact angle is very sensitive to the scale (Figure 2). The best way to measure the contact angle on a well-defined scale is to compare theoretical droplet shapes (numerical solutions of the Young–Laplace equation) subject to the initial condition set by the contact angle with the fluorescence images of monolayer droplets. The contact angle is the fit parameter in this droplet-fitting procedure.

The Young–Laplace eq 5 together with Young's eq 7 depend on the set of parameters (Δ , $\lambda_{\text{LC/G}}$, $\lambda_{\text{LC/LE}}$, $\lambda_{\text{LE/G}}$, $\mu_{\text{LC/G}}$, $\mu_{\text{LE/G}}$, p). In the numerical treatment (Appendix D), the line-tension difference of the LC tensions is replaced by the contact angle, and the pressure is replaced by the area. Also, all quantities are made dimensionless (eqs 11 and 12) such that the remaining parameters are (Δ/\sqrt{A} , α , $\tilde{\lambda}_{\text{LE/G}}$, $\tilde{\mu}$).

The material parameters of the methyl octadecanoate monolayer phases used for the droplet simulation were taken from refs 29, 25, and 30 (surface potentials: $V_{\text{LC/G}} = 0.41 \text{ V}$, $V_{\text{LE/G}} = 0.145 \text{ V}$, line tension: $\lambda_{\text{LE/G}}^{\Delta=5\text{\AA}} = 0.54 \text{ pN}^{22}$).

Furthermore, we made use of the shape-invariance setting $\Delta = 1 \mu\text{m}$ (only the shape below the resolution of the images is affected by this choice). Performing a shape-invariant scale transformation from the data in the literature toward a cutoff of $\Delta = 1 \mu\text{m}$ results in the following parameters for the simulation: $\tilde{\lambda}_{\text{LE/G}} = 3.81$ (cf. eqs 8, and 11) and $\tilde{\mu} = 0.354$ (cf. eq 12). The droplet area of the experimental droplets was measured directly on the image ($A = 8.9 \times 10^{-10} \text{ m}^2$, $2.0 \times 10^{-10} \text{ m}^2$, $0.7 \times 10^{-10} \text{ m}^2$, and $0.1 \times 10^{-10} \text{ m}^2$). The corresponding simulated droplets are shown in Figure 4a. On this scale ($\Delta = 1 \mu\text{m}$), the fitted contact angle is $\alpha = 73^\circ$. With Young's eq 7, one finds $\lambda_{\text{LC/G}}^{\Delta=1\mu\text{m}} - \lambda_{\text{LC/LE}}^{\Delta=1\mu\text{m}} = 0.093$, and for the spreading coefficient

$$S = \frac{\lambda_{\text{LC/G}} - \lambda_{\text{LC/LE}} - \lambda_{\text{LE/G}}}{\lambda_{\text{LE/G}}} \quad (14)$$

It was found that $S_{\Delta=1\mu\text{m}} = -0.7$.

A visual inspection of the droplet shapes in Figures 1 and 4a shows reasonable agreement between the numerical solution and experiment. A more quantitative comparison may be obtained by measuring the ratio of lengths $P_{\text{LE/G}}/P_{\text{LE/LC}}$ of the LE/G and LE/LC boundaries (Figure 4b). The ratios $P_{\text{LE/G}}/P_{\text{LE/LC}}$ obtained from the experimental droplets agree well with those calculated by the numerical procedures for all droplet sizes. This shows

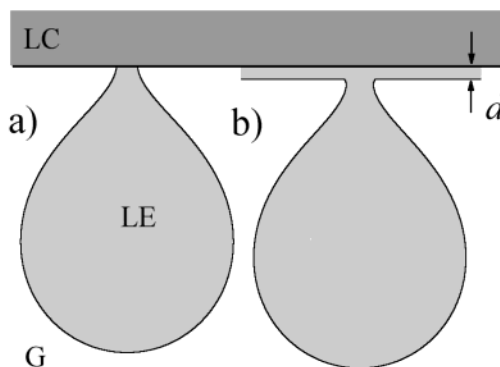


Figure 3. Sketch of a pendant LE droplet (a) partially and (b) completely (pseudopartially²³) wetting an LC/G interface. If the film thickness d of the completely wetting droplet were smaller than the optical resolution, an experimentally observed droplet could be interpreted in both ways. As shown in section 5, case b can be excluded.

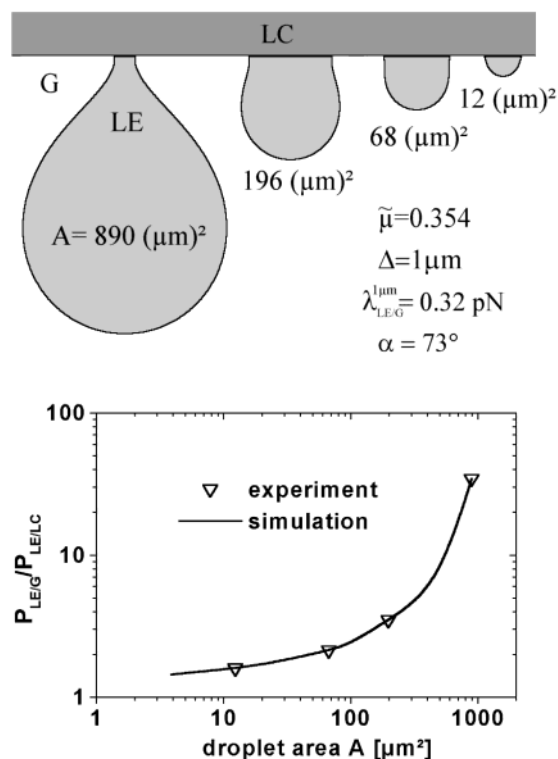


Figure 4. Top: simulated droplets using $\tilde{\mu} = 0.354$ (ref 29) and $\tilde{\lambda}_{\text{LE/G}} = 3.81$ (ref 25), $\Delta = 1 \mu\text{m}$, and the experimental areas of the droplets of Figure 1. A value of $\alpha = 73^\circ$ for the contact angle has been found by droplet fitting. Bottom: experimental (∇) and theoretical (—) values for the global wetting parameter $P_{\text{LE/G}}/P_{\text{LE/LC}}$. $P_{\text{LE/G}}/P_{\text{LE/LC}}$ diverges in the simulations as A approaches $A_{\text{dw}} \approx 10^{-9} \text{ m}^2$. For $A > A_{\text{dw}}$, droplets are globally unstable and should not be observed in experiments. Note, however, that the numerical iteration procedure used for the simulations no longer converges for $A \approx A_{\text{dw}}$ such that one can extrapolate the only value of A_{dw} .

that indeed the contact angle is a materials parameter independent of the size of the droplet.

5. Conclusions for the Cutoff Length Δ

The best fits to the experimental droplets for a different value of Δ are obtained from the numerical fits with $\Delta = 1 \mu\text{m}$ via a shape-invariant scale transformation (eqs 8 and 10). This will change the shape of the droplet only close to the LC wall, where it cannot be resolved in the experiment anyhow. The contact-angle scaling law (eq 10) predicts that the droplet with lower

Δ partially wets the LC interface with a lower (for $0 < \tilde{\mu} < 1$) contact angle. Because the contact angle is restricted to values between 0 and 180° , the scale parameter Δ also cannot be arbitrary. We have already seen in the fit of the largest experimental droplet in Figure 2b that below $\Delta_{\min} = 0.12 \mu\text{m}$ no numerical droplets could be found that fit the experimental shape. The same is true for the smaller droplets. One finds real contact angles only for Δ values larger than $\Delta_{\min} = 0.12 \mu\text{m}$. For values of $\Delta < \Delta_{\min}$, the contact angle is imaginary, and the droplet can no longer be a partially wetting droplet. Can the droplet be explained within the framework of the outlined theory with $\Delta < \Delta_{\min}$? The droplet approaching Δ_{\min} from above approaches complete wetting. Therefore, a straightforward guess is that the droplet for $\Delta < \Delta_{\min}$ can be described by a completely wetting droplet with a thin film of thickness d (Figure 3b pseudo partial wetting²³). Since we did not observe any thin films in the microscope images, the theoretical calculated film thickness d must be below the resolution of the microscope if this assumption is true. We will show in the following discussion that the theoretically predicted film thickness is larger than the microscopic resolution and that a completely wetting droplet can be excluded.

The Young–Laplace equation of a thin LE film separating an LC and a G semiplane can be solved analytically. For such a film, one finds the disjoining pressure (using eq 5) of the film to be

$$p - \frac{(\mu_{\text{LE}}^2 - \mu_{\text{G}}^2)\pi}{\Delta} = \frac{2\mu_{\text{LE/G}}\mu_{\text{LC/LE}}}{\Delta} \operatorname{arccot} \frac{d}{\Delta} \quad (15)$$

At equilibrium, this pressure is in balance with the Laplace pressure inside the droplet. We have arranged the terms in eq 15 such that the left-hand side does not change upon shape-invariant scale transformations. The Laplace pressure inside the pendant droplet can be calculated from the numerical droplet (Appendix D). For the large droplet ($A = 8.9 \times 10^{-10} \text{ m}^2$) in Figure 4, it is found to be

$$p - \frac{(\mu_i^2 - \mu_j^2)\pi}{\Delta} = 5.7 \frac{\mu_{\text{LE/G}}\mu_{\text{LC/G}}}{\sqrt{A}} \quad (16)$$

After substituting eq 16 into eq 15, one obtains the film thickness d as a function of the scale parameter Δ :

$$d = \Delta \cot \frac{5.7\Delta}{2\sqrt{A}(1 - \tilde{\mu})} \approx \frac{2\sqrt{A}(1 - \tilde{\mu})}{5.7} = 6.8 \mu\text{m} \quad (17)$$

The approximation in eq 17 holds over the whole range of the model ($\Delta \ll \sqrt{A}$). One finds that the film thickness has a value of $d = 6.8 \text{ m}$ for all scale parameters Δ . This is large enough to be observed. Because we did not observe such a film, we conclude that the droplet is a partially wetting droplet and that a three-phase intersection point exists.

Note that although Δ can be dealt with mathematically as a scale parameter that can be chosen somewhat arbitrarily there exists one well-defined physical scale Δ_r where the cross over from universal (all short-range interactions can be adsorbed into a line tension) behavior to physics determined also by the nonuniversal short-range interactions occurs. This physical Δ_r has not been measured yet; in the literature, it is set to the distance (angstroms) between the molecules. The motivation for this assumption comes from the mathematical transition from a dipole lattice to a continuous dipole distribution³¹ where the equations contain an angstrom-size Δ . Another possible inter-

pretation of the cutoff length is as the length where short-range attraction overbalances the dipole repulsion. If van der Waals forces are dominant, then the physical Δ_r would be expected to be on the order of nanometers. However, the lower limit for Δ_r determined here is 2 orders of magnitude larger—no attractive interaction known to us has this range—so we might think about another interpretation.

5.1. Pinning Effects. It might be possible that the LE droplet is pinned by some impurity to the LC substrate. If the impurity—maybe a small particle—is nonpolar and larger than $0.12 \mu\text{m}$ in diameter, then the droplet can be stably attached to the wall via the impurity. However, other observations give evidence that this is not the case. In related experiments, we disturbed the thermodynamic equilibrium using an IR laser as a heating device²⁷ and let the monolayer relax. During the procedure, the three-phase intersection points move and equilibrate very quickly ($t \approx 1 \text{ s}$). Pinning on the highly viscous LC wall would not allow this fast movement and equilibration of the droplet shape.

5.2. Surface Effect of the Phase Boundaries. We suggest an interpretation of the large Δ_r as an interfacial effect on the droplet border line. Note that the Δ that enters the Young–Laplace equation occurs only in integrals describing the electrostatic pressure on the droplet interface. With this interpretation, Δ represents a dipole correlation or healing length on the phase boundary. Previous papers^{25,29,32} report on a change of the materials parameters on phase boundaries from those in the bulk, which is consistent with this interpretation. Stability conditions lead us to suspect that the phase boundaries are not sharp by themselves but form a continuum of finite thickness. Presumably, the surface potential cannot switch from its value in the LE phase toward that in the G phase on length scales smaller than $0.1 \mu\text{m}$, as the electric fields around this transition become energetically too costly. Another explanation might be nonpolar impurities that form a kind of 1D monolayer on the “droplet surface”.

6. Results

At equilibrium, the shape of a wetting 2D droplet is determined by the Young–Laplace equation, which is similar to the 3D Young–Laplace equation with an additional electrostatic pressure term due to long-range dipole interactions. This dipole pressure term contains a scale parameter that separates between long-range dipole interactions and short-range interactions (bare line tension). The scale parameter, line tension, and pressure can be simultaneously changed by a shape-invariant scale transformation keeping invariant the Young–Laplace equation and the droplet shape not too close to the intersection point.

The contact angle is determined by Young’s condition and depends only on the bare line tensions. It is a materials parameter and is independent of the droplet size or long-range interactions with the surroundings. Because the bare line tensions are not invariant to shape-invariant scale transformations, the contact angle is also *not* invariant to shape-invariant scale transformations.

By an iteration procedure, we calculated 2D equilibrium droplets taking into account the line tension and dipole interaction between the droplets and between the droplets and the LC wall (the dipole densities and the bare line tension of the LE/G interface in methyl octadecanoate are known from previous measurements). Comparison with experimental droplets observed in a methyl octadecanoate monolayer using fluorescence microscopy showed good agreement. Fitting the contact angle (by droplet fitting) allows us to measure the spreading coefficient $S_{\Delta=1 \mu\text{m}} = -0.7$.

Restrictions on the contact angle (between 0 and 180°) result in a lower limit for the scale parameter ($\Delta > 0.12 \mu\text{m}$). We suggest an interpretation of Δ as a dipole correlation length at the phase boundaries.

Acknowledgment. We thank Professor Möhwald for generous support and stimulating discussions and R. Netz for discussions on the size of the cutoff length. Th.M.F. thanks the German Science Foundation for providing a Heisenberg fellowship. This work is supported by the German Science Foundation within the priority program “Wetting and Structure Formation at Interfaces”.

Appendix A: Variation Problem

To be able to apply the technique of variational calculus, we need to express the free energy F as a functional of the domain boundaries ($\mathbf{r}_{ij}(s_{ij})$) tangent vectors $\mathbf{t}_{ij}(s_{ij}) = d/ds_{ij} \mathbf{r}_{ij}(s_{ij})$ between the phases i and j and the three-phase intersection points \mathbf{x}_n , where we parametrize the domain boundary by its arclength s_{ij} . This can be achieved by noting that

$$\nabla \cdot \nabla' \frac{\ln(\sqrt{(\mathbf{r} - \mathbf{r}')^2 + \Delta^2} + \Delta)}{\Delta} = - \frac{1}{\sqrt{(\mathbf{r} - \mathbf{r}')^2 + \Delta^2}^3} \quad (\text{A1})$$

from which when twice applying Greens' theorem we deduce

$$F_{\text{el}} = - \sum_{\{kl\}, \{mn\}} \frac{\mu_{kl} \mu_{mn}}{2\Delta} \int_{s_{kl}=0}^{P_{kl}} \int_{s_{mn}=0}^{P_{mn}} ds_{kl} ds_{mn} \mathbf{t}_{kl} \cdot \mathbf{t}_{mn} \ln(\rho + \Delta) \quad (\text{A2})$$

where

$$\rho = \sqrt{(\mathbf{r}_{kl}(s_{kl}) - \mathbf{r}_{mn}(s_{mn}))^2 + \Delta^2}$$

The summation and integration cover all facets $\{kl\}$ and $\{mn\}$ of length P_{kl} and P_{mn} between the domains k and l (m and n). The points $\mathbf{r}_{kl}(s_{kl}) \in \partial A_k \cap \partial A_l$ at the interface are parametrized by the arclength s_{kl} . The tangent vector \mathbf{t}_{kl} is a unit vector at the interface line at point $\mathbf{r}_{kl}(s_{kl})$ with phase $k(l)$ lying to the right (left). The free-energy functional F_0 depends only on the areas A_i of the individual phases. In terms of line integrals, these areas can be expressed as

$$A_i = \sum_{j \text{ neighbors of } i} \int_0^{P_{ij}} \mathbf{r}_{ij} \cdot \Lambda \mathbf{t}_{ij} ds_{ij} \quad (\text{A3})$$

with Λ a 90° counterclockwise rotation matrix:

$$\Lambda = \begin{pmatrix} 0 & -1 \\ 1 & 0 \end{pmatrix} \quad (\text{A4})$$

A perturbation of the monolayer pattern of the form $\tilde{\mathbf{r}}_{ij} = \mathbf{r}_{ij} + \delta \mathbf{r}_{ij}$ with the constraint that all facets with endpoint \mathbf{x}_n now end in a perturbed endpoint $\tilde{\mathbf{x}}_n = \mathbf{x}_n + \delta \mathbf{x}_n$ causes a variation of the free energy given by

$$\delta F = \sum_{ij} \int_0^{P_{ij}} ds_{ij} \left(\frac{\delta F}{\delta \mathbf{r}_{ij}(s_{ij})} \right) \cdot \delta \mathbf{r}_{ij} + \sum_n \frac{\delta F}{\delta \mathbf{x}_n} \cdot \delta \mathbf{x}_n$$

A monolayer phase pattern minimizing the free energy must satisfy the condition that $\delta F = 0$ for any perturbation of the phase boundary $\delta \mathbf{r}_{ij}$ and any allowed contact-point perturbation

$\delta \mathbf{x}_n$ leading to an Euler–Lagrange representation of the Young–Laplace equation

$$0 = \frac{\delta F}{\delta \mathbf{r}_{ij}(s_{ij})} = \left(\frac{\partial F}{\partial \mathbf{r}_{ij}} - \frac{d}{ds_{ij}} \frac{\partial F}{\partial \mathbf{t}_{ij}} \right) \quad (\text{A5})$$

and to a stability condition for the three-phase intersection point

$$\frac{\delta F}{\delta \mathbf{x}_n} \cdot \delta \mathbf{x}_n = 0 \quad \text{for all possible } \delta \mathbf{x}_n \quad (\text{A6})$$

Evaluating the Euler–Lagrange equation for the ij boundary of the total model free energy leads to the Young–Laplace equation (see ref 25 for details):

$$\lambda_{ij} \kappa_{ij}(s_{ij}) = p_{ij} - \sum_{\{kl\}} \mu_{ij} \mu_{kl} \int_0^{P_{kl}} ds_{kl} \frac{\mathbf{n}_{kl} \cdot (\mathbf{r}_{ij} - \mathbf{r}_{kl})}{\Delta(\rho + \Delta)\rho} \quad (\text{A7})$$

where $\mathbf{n}_{kl} = \Lambda \mathbf{t}_{kl}$ is the unit normal vector at \mathbf{r}_{kl} pointing into phase l . Application of Green's theorem to eq A7 gives the Young–Laplace equation in a surface integral representation (eq 5).

All facets between two phases are either closed lines or they generically start and end in three-phase contact points \mathbf{x}_n ($n = 1, 2, 3, \dots$). Suppose that one of the endpoints of the facet between phases i and j is \mathbf{x}_n . Let us define

$$\sigma_{ij}^n = \begin{cases} 1 & \text{if } \mathbf{r}_{ij}(P_{ij}) = \mathbf{x}_n \\ -1 & \text{if } \mathbf{r}_{ij}(0) = \mathbf{x}_n \\ 0 & \text{if } \mathbf{x}_n \text{ is not an endpoint of } \mathbf{r}_{ij} \end{cases} \quad (\text{A8})$$

With this definition we may write

$$\frac{\delta F}{\delta \mathbf{x}_n} = \left(\sum_{\{ij\}} \sigma_{ij}^n \frac{\partial F}{\partial \mathbf{t}_{ij}} \right) \Big|_{\mathbf{x}_n} \quad (\text{A9})$$

The equilibrium condition for the contact point \mathbf{x}_n reads

$$\left(\sum_{\{ij\}} \sigma_{ij}^n \frac{\partial F}{\partial \mathbf{t}_{ij}} \right) \Big|_{\mathbf{x}_n} = 0 \quad (\text{A10})$$

if all phases are liquid phases. If one is a solid (LC) phase, then variations of the contact point are restricted to movements along the boundary of the solid $\delta \mathbf{x}_n = \delta x_n \mathbf{t}_{\text{LC}}$, with \mathbf{t}_{LC} the tangent vector of the solid interface, and the contact-point stability criterion (eq A10) reduces to

$$\left(\sum_{\{ij\}} \sigma_{ij}^n \frac{\partial F}{\partial \mathbf{t}_{ij}} \right) \Big|_{\mathbf{x}_n} \cdot \mathbf{t}_{\text{LC}} = 0 \quad (\text{A11})$$

The explicit evaluation of eq A11 is done in Appendix B.

Appendix B: Young's Equation

At the contact point, the sum over all dipole density or pressure differences between the phases separated by the lines joining vanishes:

$$\sum_{\{ij\}} \sigma_{ij}^n \mu_{ij} = 0 \quad (\text{B1})$$

and

$$\sum_{\{ij\}} \sigma_{ij}^n P_{ij} = 0 \quad (\text{B2})$$

The long-range electrostatic interactions do not affect the contact-point stability.

It is

$$\left. \frac{\partial F_{\text{el}}}{\partial \mathbf{t}_{ij}} \right|_{\mathbf{x}_n} = -\mu_{ij} \sum_{\{kl\}} \frac{\mu_{kl}}{\Delta} \int_{s_{kl}=0}^{P_{kl}} ds_{kl} \mathbf{t}_{kl} \ln(\sqrt{(\mathbf{x}_n - \mathbf{r}_{kl})^2 + \Delta^2} + \Delta) = \mu_{ij} \mathbf{y} \quad (\text{B3})$$

where \mathbf{y} is independent of the facet ij . It follows from eq B1 that

$$\sum_{\{ij\}} \sigma_{ij}^n \left. \frac{\partial F_{\text{el}}}{\partial \mathbf{t}_{ij}} \right|_{\mathbf{x}_n} = \left(\sum_{\{ij\}} \sigma_{ij}^n \mu_{ij} \right) \mathbf{y} = 0 \quad (\text{B4})$$

Similarly, we find

$$\left. \frac{\partial F_0}{\partial \mathbf{t}_{kl}} \right|_{\mathbf{x}_n} = \sum_i \frac{dF_0^i}{dA_i} \frac{\partial A_i}{\partial \mathbf{t}_{kl}} \Big|_{\mathbf{x}_n} = -\sum_i p_i (\delta_{ik} - \delta_{il}) \Lambda^{-1} \mathbf{x}_n = -p_{kl} \Lambda^{-1} \mathbf{x}_n \quad (\text{B5})$$

Because of eq B2, we conclude that

$$\left(\sum_{\{kl\}} \sigma_{kl}^n \frac{\partial F_0}{\partial \mathbf{t}_{kl}} \right) \Big|_{\mathbf{x}_n} = -\left(\sum_{\{kl\}} \sigma_{kl}^n p_{kl} \right) \Lambda^{-1} \mathbf{x}_n = 0 \quad (\text{B6})$$

Finally, we find

$$\sum_{\{ij\}} \sigma_{ij}^n \left. \frac{\partial F}{\partial \mathbf{t}_{ij}} \right|_{\mathbf{x}_n} = \sum_{\{ij\}} \sigma_{ij}^n \left. \frac{\partial F_\lambda}{\partial \mathbf{t}_{ij}} \right|_{\mathbf{x}_n} = \sum_{\{ij\}} \sigma_{ij}^n \lambda_{ij} \mathbf{t}_{ij} \Big|_{\mathbf{x}_n} \quad (\text{B7})$$

such that the stability criterion (eq A11) reads

$$\sum_{\{ij\}} \sigma_{ij}^n \lambda_{ij} \mathbf{t}_{ij} \Big|_{\mathbf{x}_n} \cdot \mathbf{t}_{\text{LC}} = 0 \quad (\text{B8})$$

which for the special case of a G/LE/LC contact point with a continuous LC boundary ($\mathbf{t}_{\text{LC/G}}|_{\mathbf{x}_n} = \mathbf{t}_{\text{LC/LE}}|_{\mathbf{x}_n} = \mathbf{t}_{\text{LC}}$) transforms into

$$\lambda_{\text{LC/G}} - \lambda_{\text{LC/LE}} - \lambda_{\text{LE/G}} \mathbf{t}_{\text{LC}} \cdot \mathbf{t}_{\text{G/LE}} = 0 \quad (\text{B9})$$

Noting that

$$\cos \alpha = \mathbf{t}_{\text{LC}} \cdot \mathbf{t}_{\text{G/LE}} \quad (\text{B10})$$

yields Young's condition (eq 7).

Appendix C: Scaling Laws

C.1 Shape-Invariant Scaling. In the theoretical model, a somewhat arbitrary distinction has been made between short-range interactions adsorbed into a bare line tension and long-range dipole–dipole interactions taken into account at length scales larger than the scale parameter Δ . The theory is constructed to explain the macroscopic shapes of domains. If such a theory makes any sense, the macroscopic shapes should not depend on the choice of scale parameter Δ , provided the typical length scale of the macroscopic shapes (the radius of

curvature of the shapes) is large compared to Δ . For a meaningful theory, there must exist a transformation from the microscopic parameters λ, p, Δ to the renormalized parameters λ^*, p^* , and Δ , where in terms of renormalized parameters the shapes are functions of the renormalized parameters only and Δ drops out of the equations. If such a transformation does not exist, then all of the macroscopic details would depend on an arbitrary choice of the parameter Δ , making the theory meaningless.

Equilibrium shapes are determined by the Young–Laplace equation—the shapes satisfy the equation

$$\frac{\delta F}{\delta \mathbf{r}_{ij}(s_{ij})} = 0 \quad (\text{C1})$$

Now take an arbitrary, not necessarily equilibrium, shape $\mathbf{r}_{ij}(s_{ij})$. Calculate the functional derivative $\delta F / \delta \mathbf{r}_{ij}(s_{ij})$. In the limit $\lim_{\kappa \Delta \rightarrow 0}$ and in terms of renormalized quantities, this functional derivative should not depend on Δ :

$$\lim_{\kappa \Delta \rightarrow 0} \frac{\partial}{\partial \Delta} \left[\left(\frac{\delta F}{\delta \mathbf{r}_{ij}(s_{ij})} \right)_{\mathbf{x}_n} \right]_{\lambda_{ij}^*, p^*} = 0 \quad (\text{C2})$$

Equation C2 is the renormalization group equation defining (up to some constants) the renormalized line tension and pressure. If it holds for any shape, then it holds for an equilibrium shape. Hence, if the functional derivative vanishes for a certain shape and set of bare parameters λ, p , and Δ , it vanishes for a whole 1D family of parameters defined by $\lambda^*(\lambda, p, \Delta) = \text{const}$ and $p^*(\lambda, p, \Delta) = \text{const}$. The shapes are independent of Δ in terms of renormalized quantities. In Appendix A and in ref 25, it is shown that

$$\frac{\delta F}{\delta \mathbf{r}_{ij}(s_{ij})} = \left[\lambda_{ij} \kappa_{ij}(s_{ij}) - p_{ij} + \sum_{\{kl\}} \mu_{ij} \mu_{kl} \int_0^{P_{kl}} ds_{kl} \frac{\mathbf{n}_{kl} \cdot (\mathbf{r}_{ij} - \mathbf{r}_{kl})}{\Delta(\rho + \Delta)\rho} \right] \mathbf{n}_{ij} \quad (\text{C3})$$

Making use of

$$\frac{1}{\Delta(\rho + \Delta)\rho} = \frac{1}{\Delta(\mathbf{r}_{kl} - \mathbf{r}_{ij})^2} - \frac{1}{\rho(\mathbf{r}_{kl} - \mathbf{r}_{ij})^2} \quad (\text{C4})$$

and the fact that

$$\nabla \cdot \frac{(\mathbf{r} - \mathbf{r}')}{(\mathbf{r} - \mathbf{r}')^2} = 2\pi \delta(\mathbf{r} - \mathbf{r}') \quad (\text{C5})$$

and taking the derivative of eq C3 with respect to Δ at fixed renormalized quantities results in

$$\frac{\partial}{\partial \Delta} \left[\left(\frac{\delta F}{\delta \mathbf{r}_{ij}(s_{ij})} \right)_{\mathbf{x}_n} \right]_{\lambda_{ij}^*, p^*} = \left[\left(\frac{\partial \lambda_{ij}}{\partial \Delta} \right) \kappa_{ij}(s_{ij}) - \left(\frac{\partial p_{ij}}{\partial \Delta} \right)_{p^*} - \frac{(\mu_i^2 - \mu_j^2)\pi}{\Delta^2} + \sum_{\{kl\}} \mu_{ij} \mu_{kl} \int_0^{P_{kl}} ds_{kl} \frac{\Delta \mathbf{n}_{kl} \cdot (\mathbf{r}_{ij} - \mathbf{r}_{kl})}{(\mathbf{r}_{ij} - \mathbf{r}_{kl})^2 \rho^3} \right] \mathbf{n}_{ij} \quad (\text{C6})$$

The integral on the right-hand side of eq C6 vanishes in the limit $\lim_{\kappa \Delta \rightarrow 0}$ provided that $(\mathbf{r}_{ij} - \mathbf{r}_{kl})^2$ remains finite everywhere. The expression $(\mathbf{r}_{ij} - \mathbf{r}_{kl})^2$ vanishes only if the ij boundary

coincides with the kl boundary (i.e., if $\mathbf{r}_{kl}(s_{kl}) = \mathbf{r}_{ij}(s'_{ij})$). We may expand the expression

$$\frac{\mathbf{n}'_{ij} \cdot (\mathbf{r}_{ij} - \mathbf{r}'_{ij})}{(\mathbf{r}_{ij} - \mathbf{r}'_{ij})^2 \rho^3} \quad (\text{C7})$$

around $\mathbf{r}_{ij}(s_{ij})$ with the result

$$\begin{aligned} \frac{\mathbf{n}' \cdot (\mathbf{r} - \mathbf{r}')}{(\mathbf{r} - \mathbf{r}')^2 \rho^3} &\approx \frac{(\mathbf{n} - \kappa(s' - s)\mathbf{t}) \cdot (- (s' - s)\mathbf{t} + \kappa/2(s' - s)^2 \mathbf{n})}{(s' - s)^2 \sqrt{(s' - s)^2 + \Delta^2}^3} \\ &= \frac{\kappa/2}{\sqrt{(s' - s)^2 + \Delta^2}^3} \end{aligned} \quad (\text{C8})$$

Inserting eq C8 into eq C6 and taking the limit $\lim_{\Delta \rightarrow 0}$ results in

$$\begin{aligned} &\lim_{\kappa\Delta \rightarrow 0} \frac{\partial}{\partial \Delta} \left[\left(\frac{\delta F}{\delta \mathbf{r}_{ij}(s_{ij})} \right)_{\mathbf{x}_n} \right]_{\lambda_{ij}^*, p^*} \\ &= \left[\left(\frac{\partial \lambda_{ij}}{\partial \Delta} \right)_{\lambda_{ij}^*} \kappa_{ij}(s_{ij}) - \left(\frac{\partial \left(p_{ij} - \frac{\pi(\mu_i^2 - \mu_j^2)}{\Delta} \right)}{\partial \Delta} \right)_{p^*} + \lim_{\kappa\Delta \rightarrow 0} \mu_{ij}^2 \int_{-1}^1 ds \frac{\Delta \kappa_{ij}/2}{\sqrt{s^2 + \Delta^2}^3} \right] \mathbf{n}_{ij} \\ &= \left[\left(\frac{\partial \lambda_{ij}}{\partial \Delta} \right)_{\lambda_{ij}^*} \kappa_{ij}(s_{ij}) - \left(\frac{\partial \left(p_{ij} - \frac{\pi(\mu_i^2 - \mu_j^2)}{\Delta} \right)}{\partial \Delta} \right)_{p^*} + \frac{\kappa_{ij} \mu_{ij}^2}{\Delta} \right] \mathbf{n}_{ij} \\ &= \left[\left(\frac{\partial (\lambda_{ij} - \mu_{ij}^2 \ln \sqrt{A/\Delta})}{\partial \Delta} \right)_{\lambda_{ij}^*} \kappa_{ij}(s_{ij}) - \left(\frac{\partial \left(p_{ij} - \frac{\pi(\mu_i^2 - \mu_j^2)}{\Delta} \right)}{\partial \Delta} \right)_{p^*} \right] \mathbf{n}_{ij} \end{aligned} \quad (\text{C9})$$

If this expression should vanish for any shape defined by κ_{ij} , as required by eq C2, both partial derivatives in the last line of eq C9 must vanish individually. It is easy to see that the definitions

$$\lambda_{ij}^* = \lambda_{ij} - \mu_{ij}^2 \ln \frac{\sqrt{A}}{\Delta} \quad (\text{C10})$$

and

$$p^* = p - \frac{(\mu_i^2 - \mu_j^2)\pi}{\Delta} \quad (\text{C11})$$

satisfy the renormalization group equation C2. A change in Δ at constant renormalized quantities does not change the shape. From this, it follows directly that eq 8 is a shape-invariant scale transformation. The shape invariance strictly holds only in the limit $\lim_{\kappa\Delta \rightarrow 0}$. At finite Δ , the shape changes when performing a shape-invariant scale transformation. The changes are most pronounced in regions where the curvature of the shape boundary is large (near the three-phase contact points), whereas far away from divergencies in the curvature the shape invariance still holds to a very good approximation.

C.2. Contact-Angle-Invariant Scaling. In Appendix B, we have shown that the boundary condition at the three-phase contact point satisfies Young's condition with the bare line tensions. Expressing Young's equation in terms of renormalized line tensions leads to an equation that is not independent of Δ .

The functional derivative of the free energy with respect to the intersection points satisfies

$$\frac{\partial}{\partial \Delta} \left[\left(\frac{\delta F}{\delta \mathbf{x}_n} \right)_{\mathbf{r}(s)} \right]_{\lambda_{ij}} = 0 \quad (\text{C12})$$

(i.e., the contact-point stability is invariant at fixed bare line tensions, not at fixed renormalized line tensions). The derivation of eq C12 from eq 7 is trivial. As a consequence of this, the total variation of the free energy cannot satisfy a renormalization group equation of the kind

$$\lim_{\kappa\Delta \rightarrow 0} \frac{\partial}{\partial \Delta} [\delta F]_{\lambda_{ij}^*, p^*} = 0 \quad (\text{C13})$$

Therefore, the entire monolayer structure depends on all three parameters λ , Δ , and p . It is the boundary condition at the three-phase intersection point where Δ reenters into the renormalized equations. This does not render the theory meaningless, as the stability condition at the contact point is clearly a microscopic condition, even if in the current frame it is an equation somewhat extrapolated from the macroscopic concept of infinitely sharp phase boundaries. Ultimately, when the dipole–dipole interaction really dominates, all droplets must dewet the phase boundaries such that no three-phase intersection points exist, and the pattern becomes completely shape-invariant under shape-invariant scale transformations. For the pendant droplet in the current paper, a droplet exceeding a maximum size must disjoin into a small droplet partially wetting the LC wall and a second disjoined droplet detaching from the wall. Indeed the droplet of size $A = 8.9 \times 10^{-10} \text{ m}^2$ is the largest partially wetting droplet ever observed in the monolayer, whereas LE droplets of a larger size are observed frequently inside the gaseous phase.

Appendix D: Numerics

Finding theoretical equilibrium droplet shapes is equivalent to finding solutions of the Young–Laplace eq 5 and Young's condition (eq 7). These two equations define a nonlinear set of integrodifferential equations and are solved numerically. The calculation time can be reduced drastically if the line-integral expression (eq A7) instead of the surface-integral representation (eq 5) is used. For further use, we transform eq A7 to remove the divergency in the integral. We consider the geometry as sketched in Figure 3a and drop the subscripts characterizing the position, tangent vector, normal vector, arclength, and curvature of the LE/G boundary, multiply eq A7 by $[\delta(s - s') - (1/P)]$, and integrate over the entire LE/G interface to obtain

$$\begin{aligned} &\lambda_{\text{LE/G}} \left(\kappa(s') - \frac{2\alpha}{P} \right) + \\ &\sum_{\{kl\}} \mu_{\text{LE/G}} \mu_{kl} \int_0^P ds \int_0^{P_{kl}} ds_{kl} \left[\delta(s - s') - \frac{1}{P} \right] \frac{\mathbf{n}_{kl} \cdot (\mathbf{r} - \mathbf{r}_{kl})}{\Delta(\rho + \Delta)\rho} = 0 \end{aligned} \quad (\text{D1})$$

where we have made use of $\kappa = d\phi/ds$ with ϕ the angle of the tangent vector with respect to some reference direction. Also, the total angular change in orientation of the LE/G interface equals twice the contact angle α with the LC boundary. After collecting the terms in eq D1 that are proportional to $\mu_{\text{LE/G}}$ and to $\mu_{\text{LC/G}}$, we might rewrite it as (using eqs 11 and 12):

$$\kappa(s) = \frac{2\alpha}{P} - \frac{\tilde{\mu}}{\tilde{\lambda}_{\text{LE/G}}} \delta I_{\text{LE}}(s) - \frac{1}{\tilde{\lambda}_{\text{LE/G}}} \delta I_{\text{LC}}(s) \quad (\text{D2})$$

The scale parameter Δ is chosen on the order of μm such that its product with the curvature remains small ($\Delta\kappa \ll 1$) but larger than the numerical integration step width ds .

The self-interaction integral I_{LE} is defined by

$$I_{LE}(s) = - \oint_{\partial A_{LE}} ds' \frac{\mathbf{n}' \cdot (\mathbf{r} - \mathbf{r}')}{(\mathbf{r} - \mathbf{r}')^2 \rho} \quad (\text{D3})$$

where we have made use of

$$\oint_{\partial A_{LE}} ds' \frac{\mathbf{n}' \cdot (\mathbf{r} - \mathbf{r}')}{\Delta(\rho + \Delta)\rho} = \frac{\pi}{\Delta} - \oint_{\partial A_{LE}} ds' \frac{\mathbf{n}' \cdot (\mathbf{r} - \mathbf{r}')}{(\mathbf{r} - \mathbf{r}')^2 \rho} \quad (\text{D4})$$

The LC droplet-interaction integral I_{LC} reads

$$\begin{aligned} I_{LC}(s) &= \int_{\text{half plane}} \frac{dA'}{\rho^3} \\ &= \frac{2}{\Delta} \operatorname{arccot} \frac{-\mathbf{n}_{LC} \cdot (\mathbf{r} - \mathbf{r}_{LC})}{\Delta} \end{aligned} \quad (\text{D5})$$

Here, \mathbf{n}_{LC} is the inward normal to the LC half-plane, and \mathbf{r}_{LC} lies on the LC interface. The integrals $\delta I_{LE}(s)$ and $\delta I_{LC}(s)$ are defined via

$$\delta I_j(s) = I_j(s) - \frac{1}{P} \int_0^P ds' I_j(s') \quad (\text{D6})$$

The simplest procedure to resolve the integrodifferential equation (eq D2) is to iterate it in the form

$$\kappa_{n+1}(s) = \frac{2\alpha}{P} - \frac{\tilde{\mu}}{\tilde{\lambda}_{LE/G}} \delta I_{LE,n}(s) - \frac{1}{\tilde{\lambda}_{LE/G}} \delta I_{LC,n}(s) \quad (\text{D7})$$

and integrate to the new shape

$$\phi_{n+1}(s) = \phi_0 + \int_0^s ds' \kappa_{n+1}(s') \quad (\text{D8})$$

$$\mathbf{t}_{n+1}(s) = \begin{pmatrix} \cos \phi_{n+1}(s) \\ \sin \phi_{n+1}(s) \end{pmatrix} \quad (\text{D9})$$

$$\mathbf{r}_{n+1}(s) = \int_0^s ds' \mathbf{t}_{n+1}(s') \quad (\text{D10})$$

$$\mathbf{n}_{n+1}(s) = \begin{pmatrix} 0 & -1 \\ 1 & 0 \end{pmatrix} \mathbf{t}_{n+1}(s) \quad (\text{D11})$$

where n denotes the iteration step. If the procedure is converging during iteration, the shape \mathbf{r}_n is approaching the final shape \mathbf{r}_∞ , fulfilling the Young–Laplace equation (eq D2). The perimeter P of the LE/G droplet interface is conserved during this procedure.

The iteration procedure showed good convergence for a large range of parameters. Starting, for instance, with $\kappa_0(s) = \text{const}$ (circle), repeated application of eqs D8–D11, D3, and D5–D7 may lead to shapes fulfilling eq D2 for a given set $(\tilde{\mu}, \tilde{\lambda}_{LE/G}, \Delta, P, \alpha)$. The iteration procedure was successful for sufficiently small droplet areas. Droplets in a parameter range where shape instabilities occur did not converge.

To replace the perimeter P by the droplet area

$$A = - \frac{1}{2} \oint_{\partial A_{LE}} ds \mathbf{r} \cdot \mathbf{n} \quad (\text{D12})$$

we applied a regula falsi iteration (i.e., the converged droplet

$\mathbf{r}(s)$ is rescaled to the target area A_0). The new droplet is taken as the initial droplet for another droplet shape iteration:

$$\tilde{\mathbf{r}}(\tilde{s}) = \gamma \mathbf{r}(\tilde{s}/\gamma) \quad (\text{D13})$$

where

$$\gamma = \sqrt{\frac{A_0}{A}} \quad (\text{D14})$$

and \tilde{s} ranges from 0 to $\tilde{P} = \gamma P$. The procedure is repeated until the droplet area A equals A_0 with sufficient precision. As a result, we obtain the droplet shape $\mathbf{r}(s)$ with perimeter P as function of the parameters $\tilde{\mu}$, $\tilde{\lambda}_{LE/G}$, Δ/\sqrt{A} , and α .

The renormalized pressure is given by

$$p^* = \frac{\mu_{LE/G} \mu_{LC/G}}{P} \left(\alpha \tilde{\lambda} + \frac{\tilde{\mu}}{2} \int_0^P ds I_{LE}(s) + \frac{1}{2} \int_0^P ds I_{LC}(s) \right) \quad (\text{D15})$$

The renormalized pressure coincides with the left-hand side in eqs 15 and 16.

References and Notes

- (1) DeGennes, P. G. *Rev. Mod. Phys.* **1985**, *57*, 827.
- (2) Young, T. *Philos. Trans. R. Soc. London* **1805**, *95*, 65.
- (3) Hagen, J. P.; McConnell, H. M. *Colloids Surf.* **1995**, *102*, 167.
- (4) Herminghaus, S.; Jakobs, K.; Mecke, K.; Bischof, J.; Fery, A.; Ibn-Elhaj, M.; Schlagowski, S. *Science (Washington, D.C.)* **1998**, *282*, 916.
- (5) Stauffer, C. E. *J. Phys. Chem.* **1965**, *69*, 1933.
- (6) Brochard-Wyart, F.; Dailant, J. *Can. J. Phys.* **1990**, *68*, 1084.
- (7) Reiter, G. *Phys. Rev. Lett.* **1992**, *68*, 75.
- (8) Khattari, Z.; Heinig, P.; Wurlitzer, S.; Steffen, P.; Lösche, M.; Fischer, Th. M. *Langmuir* **2002**, *18*, 2273.
- (9) Babcock, G. T.; Wikström, M. *Nature (London)* **1992**, *356*, 301.
- (10) Lee, J.-D.; Kravchenko, V.; Kirkland, T. N.; Han, J.; Mackman, N.; Moriarty, A.; Leturcq, D.; Tobias, P. S.; Ulevitch, R. J. *Proc. Natl. Acad. Sci. U.S.A.* **1993**, *90*, 1993.
- (11) Hofmann, K. P.; Heck, M. Light-Induced Protein–Protein Interactions on the Rod Photoreceptor Disc Membrane. In *Biomembranes*; Lee, A. G., Ed.; JAI Press: Greenwich, 1996; Vol. 2A, p 141.
- (12) Rietveld, A.; Simons, K. *Biochim. Biophys. Acta* **1998**, *1376*, 467.
- (13) McConnell, H. M. *Annu. Rev. Phys. Chem.* **1991**, *42*, 171.
- (14) de Koker, R.; McConnell, H. M. *J. Phys. Chem.* **1993**, *97*, 13419.
- (15) Lee, K. Y. C.; McConnell, H. M. *J. Phys. Chem.* **1993**, *97*, 9532.
- (16) Kaganer, V. M.; Möhwald, H.; Dutta, P. *Rev. Mod. Phys.* **1999**, *71*, 779.
- (17) Perkovic, S.; McConnell, H. M. *J. Phys. Chem B* **1997**, *101*, 381.
- (18) Seul, M.; Andelman, D. *Science (Washington, D.C.)* **1995**, *267*, 476.
- (19) Bare is an attribute to distinguish the bare parameters (λ , p , Δ) introduced here from another set of renormalized parameters (λ^* , p^* , Δ) defined in Appendix C. If we express quantities in terms of bare parameters, then Young's condition does not depend on Δ , whereas the shape does. In terms of renormalized parameters, the opposite is true—changing Δ while keeping the other renormalized quantities fixed does not change the shape, but Young's condition now depends on Δ .
- (20) Khattari, Z.; Fischer, Th. M. *J. Phys. Chem B* **2002**, *106*, 1677.
- (21) Hurley, M. M.; Singer, S. J. *J. Phys. Chem.* **1992**, *96*, 1938.
- (22) The line tension can be calculated at the scale of 5 Å; however, it has no physical meaning because it is calculated on a scale smaller than the characteristic length of the van der Waals forces. However, most measurements of the line tension in the literature are based on a postulated cutoff of 5 Å, and we need to calculate it in order to compare our values with those obtained in the literature.
- (23) Pseudo partial wetting can occur only if there exists an attractive interaction between the interfaces of a thin wetting film. As the repulsive dipole interactions within the film tends to keep all parts of the film as far apart as possible, the dipole self-energy in the LE film is lowered if the LE film gets thinner. Hence, the long-range repulsion within the film generates an attractive interaction between the LC/LE and the LE/G interfaces, which could lead to a pseudo partial wetting of the droplet.
- (24) Rivière, S.; Henon, S.; Meunier, J.; Albrecht, G.; Boissonade, M. M.; Baszkin, A. *Phys. Rev. Lett.* **1995**, *75*, 2506.
- (25) Heinig, P.; Steffen, P.; Wurlitzer, S.; Fischer, T. M. *Langmuir* **2001**, *17*, 6633.
- (26) McNutt, J. E.; Andes, J. M. *J. Chem. Phys.* **1959**, *30*, 597.

- (27) Wurlitzer, S.; Lautz, C.; Liley, M.; Duschl, C.; Fischer, Th. M. *J. Phys. Chem. B* **2001**, *105*, 182.
- (28) Lösche, M.; Sackmann, E.; Moehwald, H. *Ber. Bunsen-Ges. Phys. Chem.* **1983**, *87*, 848.
- (29) Heinig, P.; Wurlitzer, S.; Steffen, P.; Kremer, F.; Fischer, Th. M. *Langmuir* **2000**, *16*, 10254.
- (30) Wurlitzer, S.; Steffen, P.; Wurlitzer, M.; Khattari, Z.; Fischer, Th. M. *J. Chem. Phys.* **2000**, *113*, 3822.
- (31) McConnell, H. M.; Moy, V. T. *J. Phys. Chem.* **1988**, *92*, 4520.
- (32) Pandit, R.; Fisher, M. E. *Phys. Rev. Lett.* **1983**, *51*, 1772.